RESEARCH ARTICLE

Groundwater quality evaluation based on water quality indices (WQI) using GIS: Maadher plain of Hodna, Northern Algeria

Tahar Selmane[1] · Mostefa Dougha[1] · Salim Djerbouai[1] · Djamaleddine djemiat[1] · Nadjet Lemouari[2]

Abstract

In a semi-arid region of Maadher, central Hodna (Algeria), groundwater is the main source for agricultural and domestic purposes. Anthropogenic activities and the presence of climate change's effects have a significant impact on the region's groundwater quality. This study's goals were to use water quality indices to evaluate the groundwater's quality and its suitability for drinking and irrigation, as well as to identify contaminated wells using a geographic information system (GIS) and the spatial interpolation techniques of ordinary kriging and inverse distance weighting (IDW). The results reveal that all water samples exceeded the World Health Organization's standards for nitrate ions and had alarming concentrations of calcium, chlorine, and sulfate (WHO). According to Piper's diagram, the groundwater hydrochemical facies is composed of the elements sulfate–chloride-nitrate-calcium (SO_4^{2-}-$Cl^-NO_3^-$-Ca^{2+} water type). The majority of samples fall into the poor water category, slightly more than 10% fall into the very poor water category, and less than 10% fall into the good to the excellent quality category, per the water quality indices, which classify samples in a similar manner. According to irrigation water indices, every sample is suitable for irrigation. Depending on the direction of groundwater flow, the spatial distributions of Ca^{2+}, Na^+, Mg^{2+}, SO_4^{2-}, and Cl^- show that their concentrations are high north of the area and relatively low south of Maadher village (Fig. 3). Nitrate concentrations are high in the majority of samples, particularly those close to the Bousaada wadi. In most samples, particularly those close to the Bousaada wadi, nitrate levels are high. Various water quality models were described, and GIS spatial distribution maps were created using standard kriging and inverse distance weighting (IDW) techniques through selected semi-variograms predicted against measurements. To determine the origin of mineralization and the chemical processes that take place in the aquifer—which include the precipitation and dissolution of dolomite, calcite, aragonite, gypsum, anhydrite, and halite—the groundwater saturation index was calculated.

Keywords Groundwater quality · Water quality indices · Kriging method · Inverse distance Weighting (IDW) method · Saturation index · Maadher

Introduction

The arid region of Maadher is located south of the salt lake "Chott Hodna", which is almost dry all year round, in the Hodna basin. This area has exploitable shallow and deep aquifers that can be used for irrigation and domestic

purposes; as a result, overexploitation has started to develop under the influence of climate change (Selmane et al. 2022; Boudiaf et al. 2020). The Maadher aquifer serves as the main source of water for domestic and agricultural needs in the densely populated area of Bousaada, and water is supplied by pumped wells. Currently, many countries lack access to appropriate groundwater for domestic and irrigation purposes (Pazand et al. 2018; Dougha and Hasbaia 2019; Belkhiri et al. 2020).

Concerns about the region's water quality are very high because groundwater chemistry is dependent on natural geochemical processes like recharge water quality, aquifer lithology, chemical weathering of different rocks, soil gases, dissolution or precipitation reactions, ion exchange, and residence time of water in aquifers (Selmane et al. 2022;

✉ Tahar Selmane
  tahar.selmane@univ-msila.dz

1 VESDD Laboratory, University of M'sila, 28000, M'sila, Algeria

2 Scientific and Technical Research Centre On Physical and Chemical Analysis, 42004 Bou-Ismail, Tipaza, Algeria

Springer

Rashid et al. 2021). Agriculture, urban solid waste dumped next to wadi banks, and wastewater discharges are all examples of human activities that introduce undesirable elements (nitrates, pesticides, heavy metals, etc.) into groundwater and worsen its quality. Furthermore, it is unknown how sensitive the area's groundwater is to pollution (Selmane et al. 2022).

Major water contaminants in the area include a number of factors, including an excessive concentration of cations (Ca^{2+}, Mg^{2+}, Na^+) and anions (SO_4^{2-}, Cl^-, HCO_3^-, NO_3^-) (Selmane et al. 2022; Wen et al. 2013). Piper, Chadha, and Gibbs diagrams (Li et al. 2018; Rashid et al. 2020) were used to identify the types of hydrochemical waters, to confirm drinking water standards, and to provide a method for hydro-geochemical processes (mineral dissolution, ion exchange reaction, water pollution), it is necessary to analyze and interpret the quality parameters of the groundwater samples taken.

The idea of the quality index will be used to evaluate and manage water quality. Water consumption indices, such as the water quality index (WQI) and the Canadian Water Quality Index (CCME-WQI) (El Mountassir et al. 2020; Soltani et al. 2020; Li et al. 2015), as well as indices for irrigation purposes like TH (total hardness), Na% (percent sodium), and SAR (sodium adsorption ratio), will be used to assess the suitability of domestic use and irrigation (Ghazaryan et al 2020; Aravinthasamy et al. 2020; Chapman 2021). Researchers currently use these indices frequently to interpret the general quality of groundwater or surface water (Radouane et al. 2021). These indices offer qualitative values that are very useful when considering groundwater management plans that must be developed by the public authorities.

Numerous quality indices developed globally have been given the task of evaluating and controlling water quality. Horton created the first quality index in 1965 to illustrate the gradation of water quality (Radouane et al. 2021; Ramachandran et al. 2021). Recently, researchers have used it extensively to interpret the overall quality of the water, whether it be groundwater or surface water (Radouane et al. 2021; Gao et al. 2013).

The unitless water quality index (WQI) is produced by a mathematical formula that converts a substantial amount of water quality data into a manageable number (Rabeiy 2018; Bahir et al. 2020). This score illustrates how various water quality parameters collectively affect the overall water quality (Luo et al. 2018; Radouane et al. 2021). Aggregation functions, on which WQI models are based, enable the analysis of sizable data sets on water quality that change over time and space (Uddin et al. 2020a). In general, the index has been used to assess whether the particular groundwater is fit for human consumption, especially as pollution appears and the number of physicochemical parameters to be measured rises (Mutlu 2019).

The Geographic Information System (GIS) is a strong visualization tool employing distribution models to explain the spatial variation of groundwater quality parameters and indices over the study region (Hussain et al. 2017). It helps in controlling and modeling groundwater resources as well as identifying appropriate and sensitive groundwater locations. In order to create a continuous dataset for studying spatial distribution, a variety of deterministic and geostatistical interpolation techniques have been exploited, including inverse distance weighting (IDW), ordinary kriging (Taloor et al. 2020; Shil et al. 2019).

According to Obaid and Mohammed (2020), kriging is a highly regarded geostatistical interpolation technique that relies on the spatial relationships between the various measurements close to the prediction location. The approach is an estimation technique that identifies unknown values using a semivariogram and known values. Given its Gaussian assumption, the kriging prediction is the best linear unbiased estimator for spatial points (Rata et al. 2018; Rashid et al. 2019).

Many researchers have recently been interested in the accuracy of various spatial interpolation techniques for the prediction of water quality parameters (Javed et al. 2017; Gunarathna et al. 2016). Since in geostatic ordinary kriging modeling, the main parameters are spontaneously simulated with under-adjustments and the error predictions are presented by semi-variogram estimation, ordinary kriging is considered a modern and superior technique with more advantages over conventional methods (Kumar et al. 2019).

With the help of WQI indices, this study will identify the physico-chemical parameters that influence water quality and explain how they relate to one another. The limitation of areas sensitive to pollution controlled by anthropogenic factors will be achieved by using ordinary kriging and inverse distance weighting (IDW) methods to determine the spatial distribution of the main parameters.

These methods will be used for the first time to evaluate the quality of groundwater in the Maadher region of Bousaada, mainly because they make it possible to gather precise data on the water's quality and the presence of pollution zones.

Materials and methods

The methodology designed for this research work includes four main phases: laboratory analysis, verification of results, calculation of water quality indices, and finally the generation of spatial distribution maps using the ordinary kriging method. The methodology adopted for the study is presented in the flowchart, see Fig. 1.

Fig. 1 Flowchart showing the methodology adopted in this study
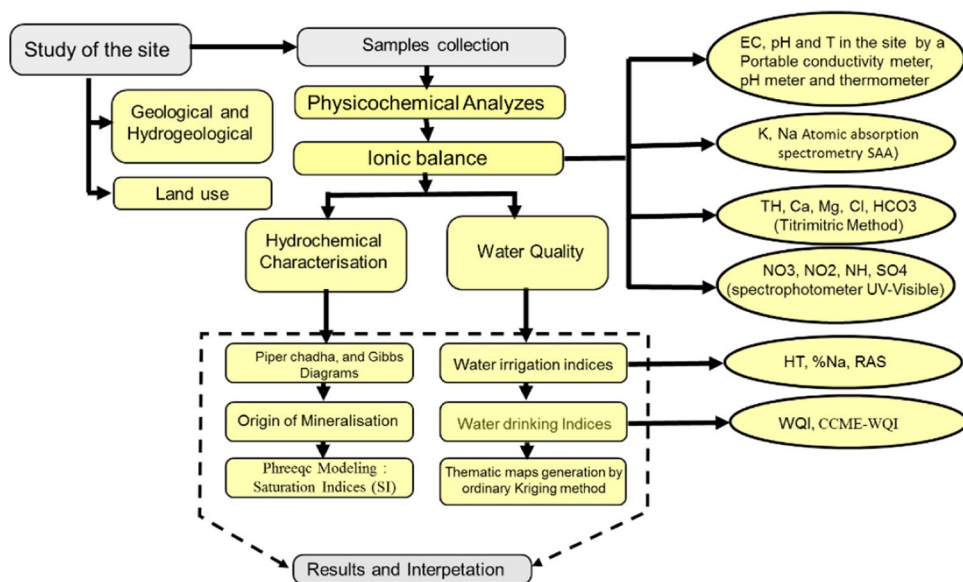
Study area

The Maadher plain is located in the Hodna basin, south of the chott, see Fig. 2. This plain of Maadher is geographically located at the coordinates of 35°17′13.39″ N, latitude and 4°16′5.81″ E, longitude with an average altitude of 450 m above sea level (Fig. 3c). Morphologically, the study area is made up of sand dunes and recent alluvial deposits and isolated rocky hills (Aissaoui 1989). The region is permanently subject to wind erosion due to the sandy texture and the lack of natural vegetation cover.

Topographically, the study area is approximately 42,000 ha which is limited in the north and the northeast by Chott Hodna and in the south and the southwest by mount Kerdada, Maalleg, Tsegna, Mabakhira, and Gharhor.

Climatically, the region has an arid to semi-arid climate, which is characterized by a cool and humid season in winter and a hot and dry season in summer. Low and poorly distributed rainfall throughout the year and variable from year to year (Boudjemline and Semar 2018), the mean annual rainfall is estimated to be 225 mm and the mean monthly temperature is 21.9 °C.

For the hydrography of the study area, three wadis are considered, i.e., Bousaada, Roumana, and Maîter. The first two wadis drain to the depression of the region and the third wadi of Maîter drains to the chott, whose waters only arrive in times of flood (Fig. 2). All these wadis contribute to the recharge of the water table. Since the 1970s, the plain of Maadher has become a large agricultural area irrigated by the pumping of groundwater. The soils are brown and reddish-brown sandy clay which allow them to be cultivated (Selmane et al. 2022). Farmers' wells have depths varying between 30 and 120 m, of which the majority of these wells do not respect the criteria of equipment and

isolation of poor water quality aquifers. The urban areas are located in the capital of the commune of Bousaada and the Maadher village.

Different geological studies carried out show the following the Triassic appears to the south of the mountains of the Hodna basin and the Cretaceous limestone occurs to the south and north of the basin (Fig. 3a); the Miocene sandstone is transgressed in the Cretaceous. Carbonate deposits fill the southern areas of the mountain range; the Lower Eocene is composed of gypsum marls, phosphate limestone, and flint limestone (Askri et al. 1995). The quaternary accumulates in the center of the basin and rests on a marly substrate.

The geometry of the Mio-Plio-Quaternary aquifer exceeds 250 m in thickness at the center of the plain (Derekov 1973; Guiraud 1973). Thus, the stratigraphy of the study area contains several alternations, often disordered, of clays, sandy clays, sandstone or sometimes clayey sands and conglomerates at the top. The main aquifers in the study area are conglomerates and sandy formations of the continental Mio-Pliocene, which communicate with all the permeable formations of the Cretaceous, of which the most important is the Albian (Guiraud 1970). The latter has a large cistern that extends to the west, where it outcrops at higher altitudes, where aquifer recharge takes place. The water table supplied mainly by infiltration of water wadi and irrigation water. The separation layer between the phreatic aquifer and the deep aquifer is defective and fissured, so that the aquifers can communicate with each other (Abdesselam et al. 2013). Since the 1970s, a drop in the groundwater level of more than 15 m has been recorded (ANRH 2006).

Groundwater in the water table (Quaternary) has a relatively high salinity compared to that in the deep aquifer. The deep aquifer (Pliocene and Miocene) consists of marls
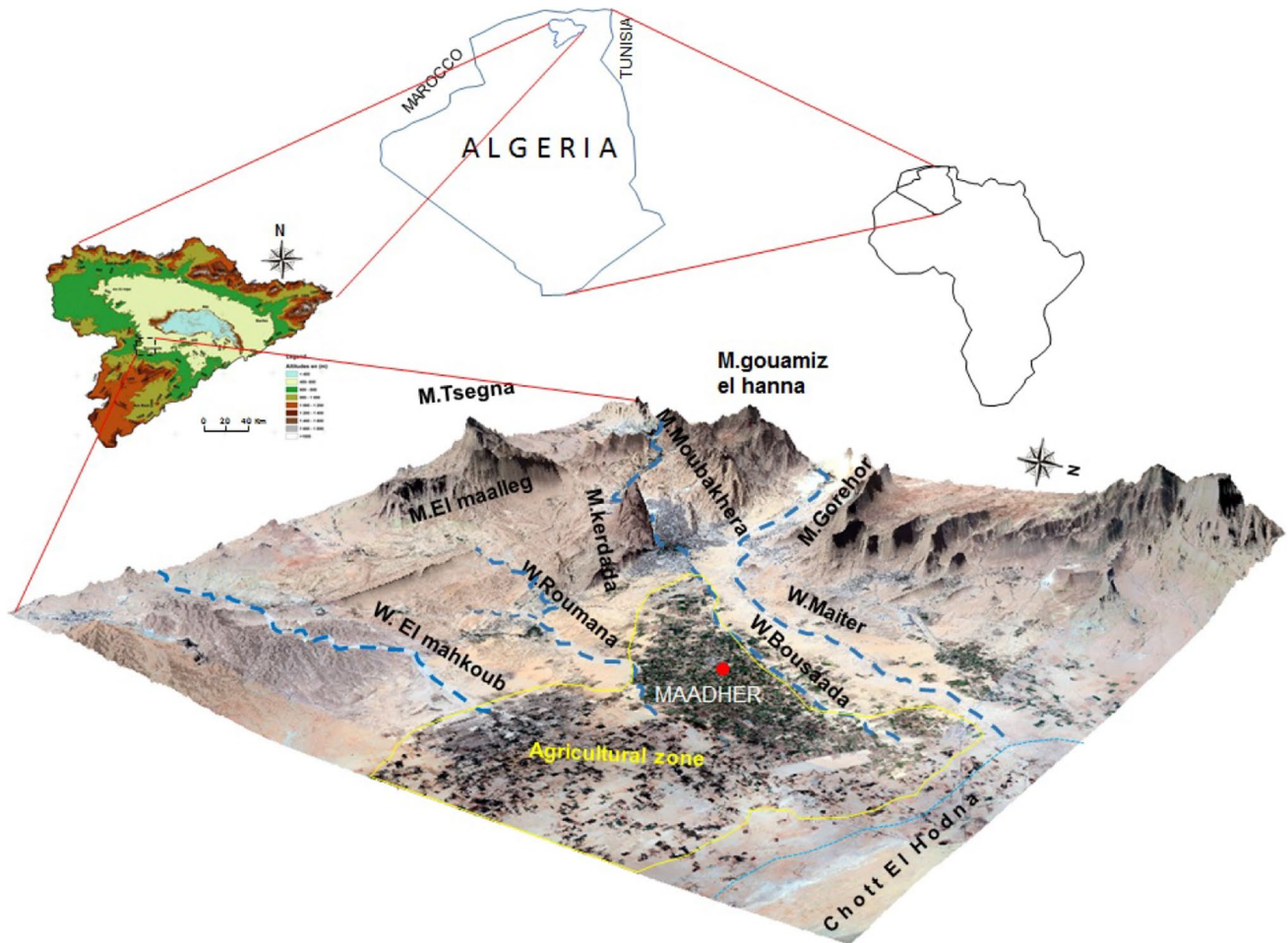
Fig. 2 Geographical position of the study area

and intercalated conglomerates (Continental Tertiary); it is a renewable aquifer (Derekov 1973; ANRH 2006).

Sampling and collecting

The representative water samples from farmers' wells were collected from the study area for the analysis of major anions and cations.

The samples were collected following the standard methods of sampling protocol (Wilde 2010).

Water samples from 33 wells were taken in clean polyethylene bottles after every 10 to 15 min of pumping, the sampling campaign is made from 17 to 20 November 2021. Temperature, electrical conductivity (EC), and pH were measured in the site by WTW cond 3110. For the analysis of major ions, the samples were immediately transferred to the University Laboratory. Calcium (Ca^{2+}), magnesium (Mg^{2+}), bicarbonate (HCO_3^-), and chloride (Cl^-) were analyzed by volumetric titration. The concentrations of Ca^{2+} and Mg^{2+} were estimated by titrimetry using 0.01 N EDTA,

and those of HCO_3^- and Cl^- by HCl and $AgNO_3$, respectively. The sodium (Na^+) and potassium (K^+) concentrations were measured using Atomic Absorption Systems Agilent technologies 200 series AA and that of the sulfate (SO_4^{2-}), ammonium (NH_4^+), nitrite (NO_2^-), and nitrates (NO_3^-) were analyzed calorimetrically with visible UV/vis ODYSSEY DR 2500 spectrophotometry. For each analysis of the parameters, the measurement is repeated at least twice.

The analyzed water chemistry data was used to determine the water quality variables in the study area and to know the quality index and to visualize the major ions of quality using the kriging method.

Water drinking indices

Water quality index (WQI)

Over the past few decades, the WQI has been considered as an effective tool that provides information on the quality of water for use by citizens and has been utilized in surface
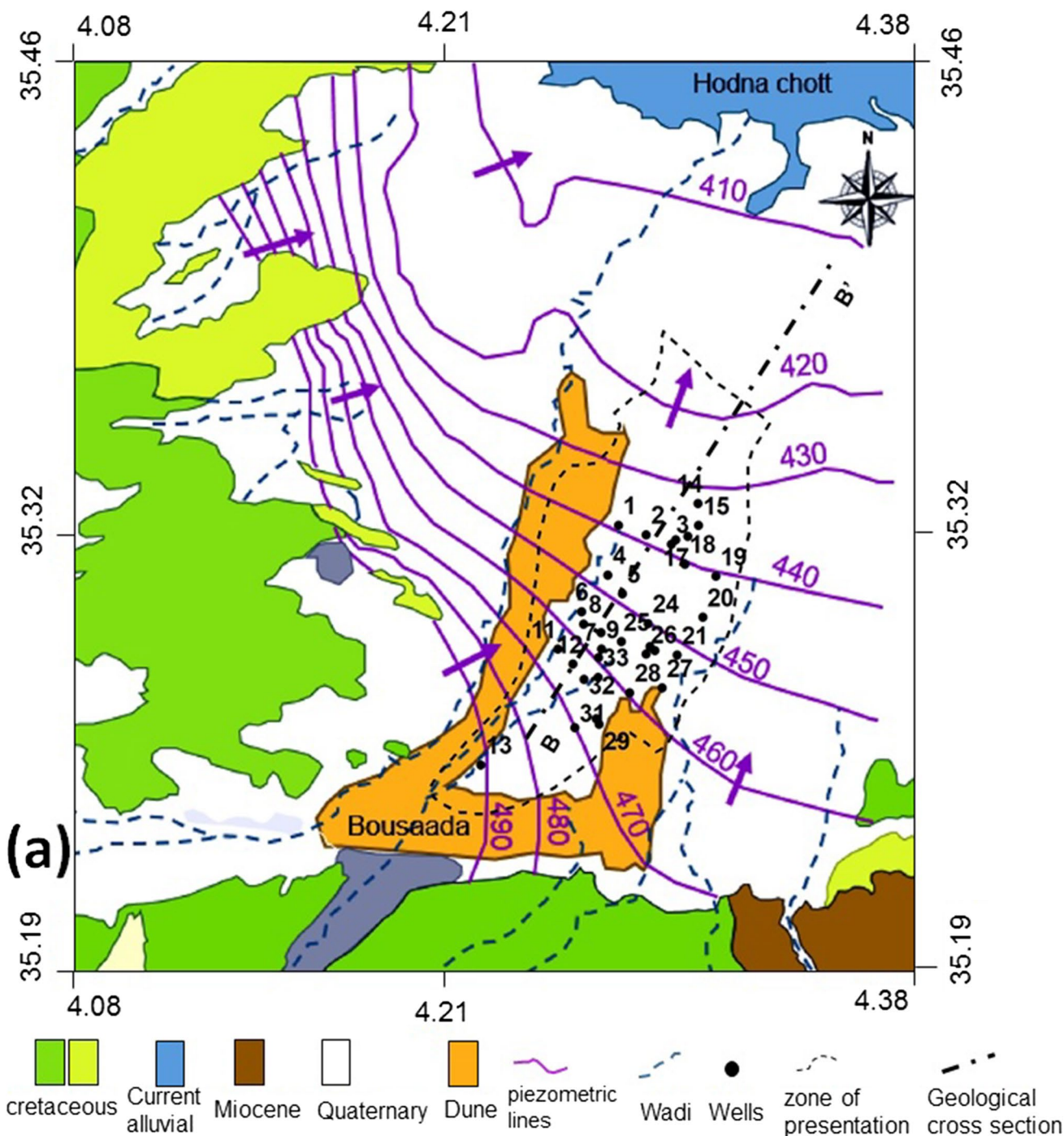
Fig. 3 Geological map with position of wells, hydrogeological cross-section along B-B' axis with elevation map of the study area

and groundwater quality evaluation (El-Zeiny and Elbeih 2019). The WQI indicates the water quality in terms of an index number which represents the overall quality of water in relation to specific standards for specific uses. WQI is defined as a rating reflecting the overall effect of various water quality parameters.

The WQI is considered a rapid and systematic tool for the evaluation and classification of water characteristics (El Mountassir et al. 2020). This indicator is calculated by the weighted output of selected parameters, and from the result obtained, the quality of the water body is classified between poor and
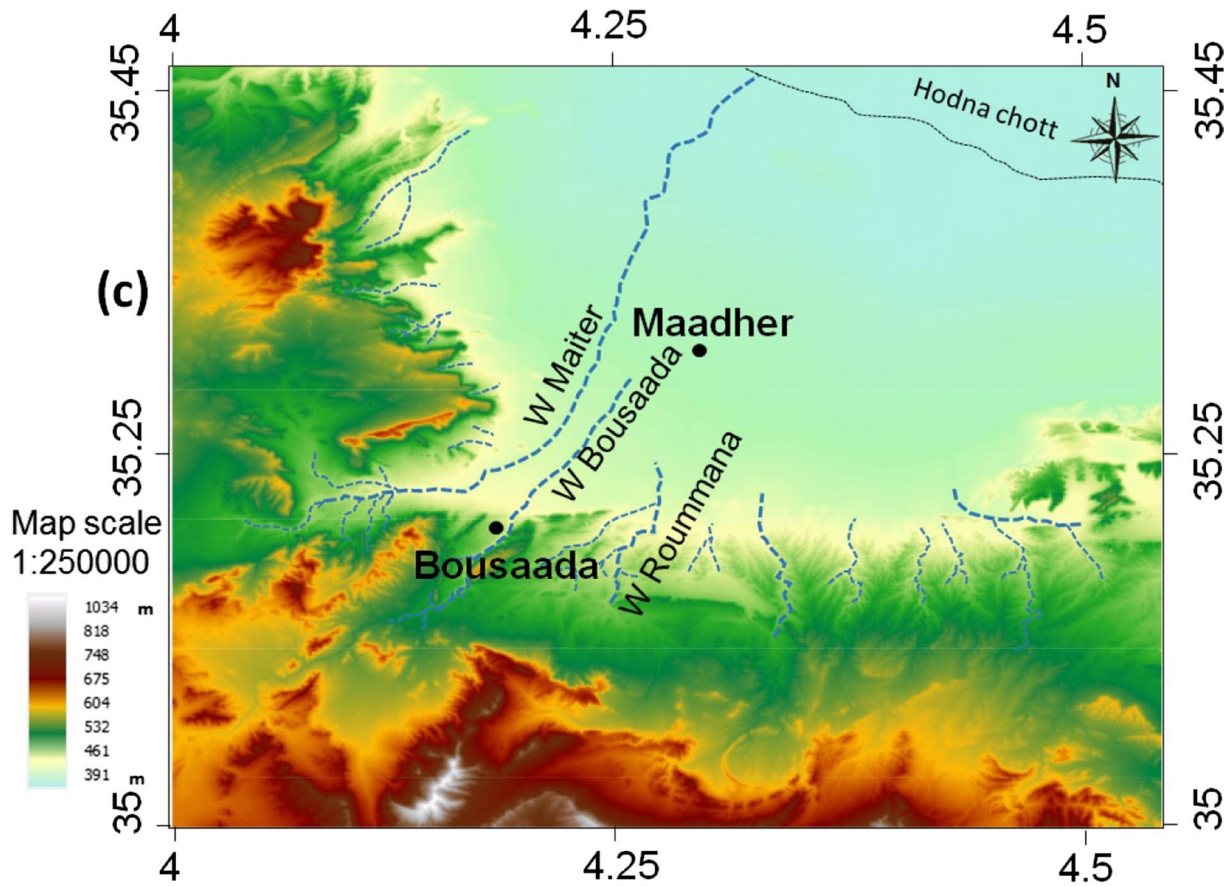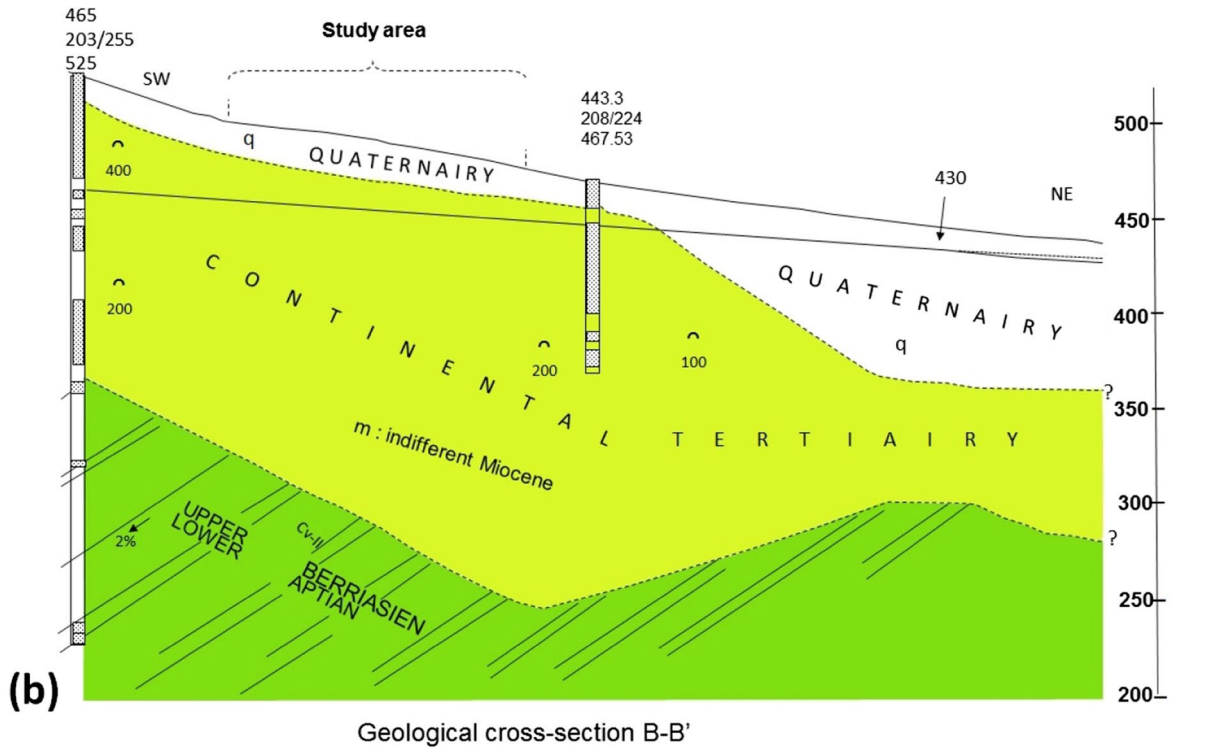
(b) Geological cross-section B-B'

(c)

Fig. 3 (continued)

optimal, relating a range of WQI variation (0–100). Several techniques can be used to monitor environmental factors.

The weighted arithmetic water quality index was used. It can be calculated using eleven measured variables from each sample taken of well water from the Maadher plain. The index calculation steps are followed, first a weight W_i is assigned from 1 to 5 for each of the parameters (pH, EC, Ca^{2+}, Mg^{2+}, HCO_3^-, Cl^-, SO_4^{2-}, TH, NO_3^-, Na^+, K^+, and NO_2^-) according to their importance in quality. For drinking water, the values of W_i are given in Table 1 (Oseke et al. 2021).

Relative weight (RW) of the water quality parameters was computed using Eq. (1) and n is the number of parameters

$$RW_i = \frac{W_i}{\sum_{i=1}^{n} W_i} \tag{1}$$

The quality rating scale for each parameter was calculated by dividing its concentration in each water sample by its respective standards according to WHO (2011) and multiplying the results by 100

$$q_i = \frac{C_i}{S_1} \times 100 \tag{2}$$

q_i is the quality rating scale. C_i is the concentration of each chemical parameter in each sample mg/l. S_i is the World Health Organization standard for each chemical parameter in mg/l according to the guidelines of the WHO (2011).

Then, for deriving the WQI value, the water quality sub-index (SI_i) for each parameter is calculated using Eq. (3)

$$SI_i = RW_i \times q_i \tag{3}$$

Finally, water quality index WQI is calculated by the use water quality sub-index (SI_i)

$$WQI = \sum_{i=1}^{n} SI_i \tag{4}$$

WQI results are evaluated into five types of water: excellent water (WQI < 50), good water (WQI = 50–100), poor water (WQI = 100–200), very poor water (WQI = 200–300), and water unsuitable for drinking (WQI > 300).

Canadian water quality index (CCME-WQI)

The CCME-WQI has been developed and modified by the Canadian Council of Ministers of the Environment (CCME 2017). This index combines three measures of variance (scope, frequency, and amplitude) to generate a single dimensionless number that represents water quality relative to the objectives and is easily understood by the public (CCME 2017). The CCME-WQI models do not require giving weight values to estimate the final result. It has been widely used in many countries to evaluate and control water quality in various uses (Soltani et al. 2020). The CCME-WQI has been used for groundwater classification because of its flexibility with respect to type, number of water quality variables, application period, and type of water (groundwater, lake, river, stream, etc.) (Yilma et al. 2018).

CCME-WQI has three factors: scope (F1), frequency (F2), and amplitude (F3). These factors are expressed as follows: F1 (scope): represents the percentage of variables that do not meet their objectives at least once during the period under consideration ("failed variables"), relative to the total number of variables measured (Eq. 5):

$$F1 = \left(\frac{\text{Number } of \text{ failed variables}}{\text{Total number of variables}} \right) \times 100 \tag{5}$$

F2 (frequency): represents the percentage of individual tests that do not meet the objectives (Eq. 6):

$$F2 = \left(\frac{\text{Number of failed tests}}{\text{Total number of variables}} \right) \times 100 \tag{6}$$

F3 (amplitude): represents the amount by which the failed test values do not meet their objectives. F3 is calculated in three steps:

Step 1: The number of times by which an individual concentration is greater than (or less than, when the objective is a minimum) the objective is termed an "excursion" and is expressed as follows in Eqs. 7 and 8. When the test value must not exceed the objective:

$$\text{Excursion}_i = \left(\frac{\text{Failed test value}_i}{\text{Objective}_j} \right) - 1 \tag{7}$$

For the cases in which the test value must not fall below the objective:

$$\text{Excursion}_i = \left(\frac{\text{Objective}_j}{\text{Failed test value}_i} \right) - 1 \tag{8}$$

Step 2: The collective amount by which individual tests are out of compliance. This is calculated by summing the excursions of individual tests from their objectives and dividing by the total number of tests (both those meeting objectives and

Table 1 Weight and relative weight of each parameter used for the WQI calculation

Parameter	pH	EC	Ca^{2+}	Mg^{2+}	HCO_3^-	Cl^-	SO_4^{2-}	TH	NO_3^-	Na^+	K^+	NO_2^-	$\sum W_i$
W_i	4	5	2	2	2	3	5	2	5	2	2	3	37
RW_I	0.11	0.14	0.05	0.05	0.05	0.08	0.14	0.05	0.14	0.05	0.05	0.08	1

those not meeting objectives). This variable, referred to as the normalized sum of excursions (NSE), is calculated as follows:

$$NSE = \frac{\sum_{i=1}^{n} \text{Excursion}_i}{\text{Number of tests}} \tag{9}$$

Step 3: F3 is then calculated by an asymptotic function that scales the normalized sum of the excursions from objectives (NSE) to yield a value between 0 and 100 (Eq. 10).

$$F_3 = \left(\frac{NSE}{0.01 \ NSE + 0.01} \right) \tag{10}$$

The CCME-WQI is finally calculated as expressed in Eq. 11

$$CCME \ WQI = 100 - \left(\frac{\sqrt{F_1^2 + F_2^2 + F_3^2}}{\sqrt{100^2 + 100^2 + 100^2}} \right) \tag{11}$$

After the CCME-WQI value was determined for the groundwater of Maadher plain using the WHO 2011 standard, water quality is categorized by linking it to one of the following five categories: excellent (95–100), good (80–94), fair (60–79), marginal (45–59) and poor (0–44).

Water irrigation indices

Irrigation suitability assessment different ionic parameters (in meq/l) were used to assess the irrigation water quality basing on various indices such as TH (total hardness), Na% (percent sodium), and SAR (alkalinity hazard) (Ghazaryan et al 2020; Aravinthasamy et al. 2020; Chapman 2021).

$$TH = 2.5 \times Ca^{2+} + 4.1 \times Mg^{2+} \tag{12}$$

$$\%Na = 100 \times \frac{Na^+ + K^+}{Na^+ + Mg^{2+} + Ca^{2+}} \tag{13}$$

$$SAR = \frac{Na^+}{\sqrt{\frac{Mg^{2+} + Ca^{2+}}{2}}} \tag{14}$$

Ordinary kriging method

The kriging method is based on the hypothesis that a spatial autocorrelation exists between the measured points in an ensemble of data. The method statistically assesses the values of the points that are regrouped automatically by a central primary variable in order to predict a continuous surface that estimates the non-measured values of other emplacements. The possible statistics are derived from a semivariogram, which is a model that evaluates the spatial

correlation gradient as a function of the distance between the donor points (Uddin et al. 2020b).

Kriging tool similar to inverse distance weighting (IDW), its general mathematics formula is

$$\widehat{Z}(S_0) = \sum_{i=1}^{N} \lambda_i Z(S_i) \tag{15}$$

$\widehat{Z}(S_0)$ is the estimated value at the location S_0, $Z(S_i)$ the measured value at the ith location, λ_i an unknown weight for the measured value at the ith location and N the number of measured values. Ordinary kriging is an estimation technique based on spatially dependent variance, which allows to find the best linear unbiased estimate (Belkhiri et al. 2020). The great advantage is using information from the semivariogram. The predictions are based on the model:

$$Z(s) = \mu + \varepsilon'(s) \tag{16}$$

where μ is an unknown constant, and is the spatially correlated stochastic part of the variation (Singh and Verma 2019).

The spatial dependence between nearby observations could be determined with the variogram, which is half the variance of the difference between the attribute values at all points separated by h as follows:

$$\widehat{\gamma}(h) = \frac{1}{2N(h)} \sum_{i=1}^{N(h)} [Z(\mu_i + h) - Z(\mu_i)]^2 \tag{17}$$

where, $\widehat{\gamma}(h)$ is the variogram for the distance h; $N(h)$ represents the number of data pairs for this offset h, and $Z(\mu_i)$ and $Z(\mu_i + h)$ are the values of the regionalized variable of interest at the location μ_i and $\mu_i + h$, respectively (Rostami et al. 2020).

Inverse distance weighted method (IDW)

A linear combination of values at known points is used to explicitly calculate the in-the-art-unknown (IDW) values, which is a deterministic estimation interpolation (Singh and Verma, 2019). According to the IDW method, each entry point has a local influence which decreases as one moves further away (Taloor et al. 2020). Neighborhood search of IDW points with power function weighting. The impact of more distant points frequently decreases as the power increases. Weight is distributed more evenly between nearby points when there is less power (Shil et al. 2019). IDW is sensitive to outliers and works best with evenly distributed points. IDW works best when the sampling is dense enough to simulate local variation. The IDW method does not explicitly assume anything about the statistical characteristics of the input data, unlike the kriging methods. When the input data does not meet the statistical presumptions of

the most sophisticated interpolation techniques, IDW is frequently used.

However, the weights $(\lambda_i(S_0))$ were estimated through inverse distance from all points to the new points by applying Eq. (18)

$$\lambda_i(S_0) = \frac{\frac{1}{\beta d(S_0,S_1)}}{\sum_{i=1}^{n} \frac{1}{\beta d(S_0,S_1)}}; \beta > 1 \qquad (18)$$

where λ_i is the weight for neighbor i (the sum of weights must be unity to ensure an unbiased interpolator), $d(S_0,S_1)$ is the distance from the new point to a known sample point, β is the coefficient used to adjust the weights, and n is the total number of points in the neighborhood analysis.

These two chosen interpolation techniques were exploited using ArcGIS 10.8 software.

Saturation index (SI)

Underground rocks contribute to the formation of water quality through ion exchange during its passage or residence in it (Jalees et al. 2021). Their total essentially equals the mineral's solubility, and SI is utilized to determine whether it is out of equilibrium or not (Jampani et al. 2020).

Geochemical modeling PHREEQC interactive version 3.4 was developed for determining and simulating hydrogeochemistry. It produces as output chemical speciation and saturation indices of chemical species. The software performs a wide range of low-temperature aqueous geochemical computations and simulates a number of reactions and processes in natural waters and laboratory studies (Lu et al. 2022; Kim and Lee 2022; Hu et al. 2021). Furthermore, the model offers information about a solution's speciation, saturation, and oxidation/reduction, which is the first step in interpreting water chemistry using a thermodynamic approach (Abdelshafy et al. 2019). The SI is a common index used for hydrogeochemical studies that describe the quantitative deviation of water from equilibrium and identifies controlling geochemical reactions (Ahmad et al. 2019). To calculate the saturation, the ionic concentrations of all the main parameters specified in the water were used (Jalees et al. 2021) and are obtained from the equation:

$$SI = log\left(\frac{IAP}{K_t}\right) \qquad (19)$$

where IAP is the ion activity product of the dissociated chemical species in solution, K_t is the equilibrium solubility product for the chemical involved at the sample temperature.

If $SI > 0$, then this indicates that the groundwater has reached the stage of oversaturation. At this point, no more minerals will be dissolved in water, resulting precipitation condition of minerals. If $SI < 0$, groundwater tends to dissolve more minerals, which leads to the dissolution condition of minerals. (Jalees et al. 2021; Ahmad et al. 2019). An SI equal 0 (with ± 0.5) indicates equilibrium conditions.

Results and discussion

Hydrogeochemical parameters of groundwater

Calculating the absolute ion balance provides information about the analytical ion measurement's accuracy (IB). A charge balance error of less than 6% exists in every sample. The majority of sample analysis results revealed respectable precision (Panneerselvam et al. 2021).

In Table 2, the result shows that the groundwater pH is between 7.34 and 8.15 for an average of 7.63. All samples fall within the scope of the WHO for drinking water. Groundwater's electrical conductivity (EC) ranges from 1035.8 to 4901.8 µS/cm, with an average of 2621.57 µS/cm, all samples exceed the recommended value WHO 1500 µS/cm except the well 13. When the water is full of minerals, the EC is generally high. The calcium (Ca^{2+}) concentration ranges from 108.6 to 601.2 mg/l, with an average of 310.52 mg/l. All samples exceed the WHO recommended limit of 75 mg/l, and they are the most abundant cation in all samples. 67.64% of the magnesium (Mg^{2+}) concentrations in all samples were within the WHO standard for drinking water 100 mg/l. Its value ranges from 36.45 to 255.20 mg/l. The average value of sodium (Na^+) is 126.35 mg/l, with a range of 42.77 to 379.06 mg/l. Potassium (K^+) levels in groundwater samples range from 5.1 to 16 mg/l, with an average of 7.3 mg/l.

The cation analysis reveals that Ca^{2+} comes first, followed by Na^+, Mg^{2+}, and finally K^+ respectively in order of importance.

The sulfate (SO_4^{2-}) is the most abundant anion in the samples analyzed, their content ranges from 250 to 1300 mg/l for an average of 659.05 mg/l. All samples are out of the standard limits for drinking water 250 mg/l. As for the chlorides (Cl^-), their content is between 88.75 and 923 mg/l, with an average of 419.31 mg/l. It was 70.58% of all samples outside the standards limits of WHO. The concentration of bicarbonate HCO_3^- in all samples was within the limits permitted by the WHO (2011) for drinking water 300 mg/l. Its values range from 149.45 to 244 mg/l and the average is 179.68 mg/l.

For nitrate, which is a pollution factor for water, 67.64% of all samples were above the acceptable value by WHO 2011 (50 mg/l), except wells 12, 13, 15, and 26 containing concentrations below 50 mg/l.

As a result, sulfate dominates the average anions content in groundwater, followed by chlorides, bicarbonate, and ultimately nitrates, in the order $SO_4^{2-} > Cl^- > HCO_3^- > NO_3^-$.

Table 2 Statistical description of the physicochemical results of samples studied

Variable	Algerian standard (2011)	WHO standard (2011)	Min	Max	Mean $\pm$ SD
T (°C)	25	-	14.80	15.80	15.29 ± 0.29
pH	6.5–9.0	8.5	7.34	8.15	7.64 ± 0.16
EC	2800	1500	1035.81	4901.78	2648.33 ± 871.21
Ca^{2+}	200	75	108.22	601.20	314.12 ± 116.20
Mg^{2+}	150	100	36.46	255.20	97.57 ± 45.55
HCO_3^-	-	300	149.45	244.00	178.84 ± 27.64
Cl^-	500	250	88.75	923.00	425.89 ± 220.68
SO_4^{2-}	400	250	250.00	1300.00	666.15 ± 232.38
TH	200	500	420.00	2450.00	1203.64 ± 471.94
NO_3^-	50	50	12.00	407.00	173.47 ± 104.41
Na^+	200	200	42.78	379.07	127.52 ± 75.73
K^+	12	12	5.10	16.00	7.35 ± 1.90
NO_2^-	0.2	3	0.00	0.02	0.00 ± 0.01
NH_4^+	0.5	1.5	0.00	0.00	0.00 ± 0.00

All parameters in mg/l except, EC (25 °C) in µs/cm, T in °C, and pH without unitters

In addition, moreover, strong linear correlations are mentioned between EC and Ca^{2+} ($R = 0.97$), Cl^- ($R = 0.95$), SO_4^{2-} ($R = 0.84$), Na^+ ($R = 0.70$), Mg^{2+} ($R = 0.66$), see Table 3. The calcium has a fort correlation with Cl^- ($R = 0.93$), SO_4^{2-} ($R = 0.78$), Mg^{2+} ($R = 0.63$) and a moderate correlation with Na^+ ($R = 0.56$) and K^+ ($R = 0.50$). On the other hand, Na^+ and K^+ ions have moderate correlations with Ca^{2+}, Cl^-, and SO_4^{2-}. As for nitrates, nitrites and bicarbonate, it was observed that they do not have good correlations with the rest of the parame.

Hydrogeochemical water classification using piper diagram

The term hydrochemical facies is used to describe the various groundwater families and the predominant chemical parameters in an aquifer, which differ in their chemical composition. The main ionic species present in most natural waters are Ca^{2+}, Mg^{2+}, Cl^-, SO_4^{2-}, Na^+, K^+, HCO_3^-, and NO_3^- (Fetter 2018). The Piper diagram has been widely used to show water classifications and water quality trends for groups of samples (Li et al. 2018).

The Piper diagram (Fig. 4) shows that the water coming from all wells contains a low percentage of $CO_3^{2-} + HCO_3^-$ (about 10%), while the percentage of $Cl^- + NO_3^-$ ranges from 40 to 70% except the wells 13, 26 contains a low percentage less than 40%. The sulfate ratios are average, ranging between 40 and 55% in most of the samples except the wells 7, 8, 11, 18, 19, 21, 22, and 30 are less than 40%.

As for the diagram of cations was observed, all samples contain a high percentage of calcium more than 50% and a

Table 3 Correlation matrix of the physicochemical parameters

Variables	T	pH	EC	Ca^{2+}	Mg^{2+}	HCO_3^-	Cl^-	SO_4^{2-}	TH	NO_3^-	Na^+	K^+	NO_2^-
T	**1**												
pH	0.17	**1**											
EC	0.22	−0.30	**1**										
Ca^{2+}	0.19	−0.23	**0.97**	**1**									
Mg^{2+}	0.04	−0.31	**0.66**	**0.63**	**1**								
HCO_3^-	−0.14	−0.30	−0.24	−0.29	−0.22	**1**							
Cl^-	0.22	−0.32	**0.95**	**0.93**	**0.65**	−0.28	**1**						
SO_4^{2-}	0.09	−0.30	**0.84**	**0.78**	**0.74**	−0.10	**0.70**	**1**					
TH	0.09	−0.19	**0.89**	**0.91**	**0.79**	−0.32	**0.83**	**0.83**	**1**				
NO_3^-	0.17	0.13	0.11	0.18	−0.03	−0.41	0.11	−0.24	0.14	**1**			
Na^+	0.15	−00.31	**0.70**	**0.56**	0.30	−0.04	**0.59**	**0.69**	**0.50**	−0.10	**1**		
K^+	0.07	0.36	0.47	**0.50**	0.29	−0.23	0.37	**0.52**	**0.55**	0.11	0.37	**1**	
NO_2^-	0.09	0.43	0.03	0.13	0.08	−0.15	−0.04	0.10	0.28	0.28	−0.22	0.45	**1**

All parameters in mg/l except, EC (25 °C) in µs/cm, T in °C, and pH without unit
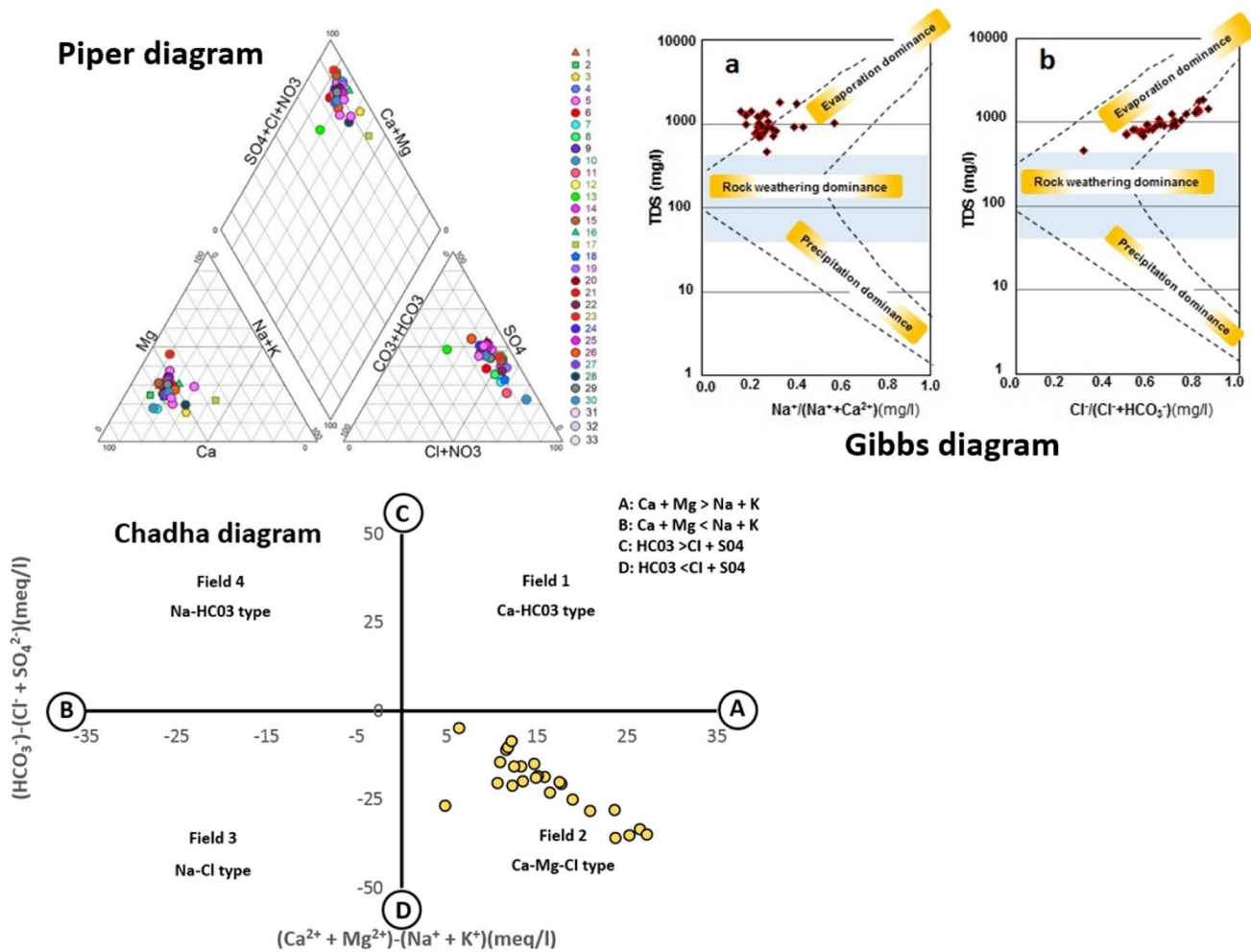
Fig. 4 Piper, Gibbs, and Chadha diagrams of the groundwater samples

low percentage of Mg^{2+} and $Na^+ + K^+$. We can say that calcium is clearly dominant compared to Mg^{2+}, Na^+, and K^+.

Also, the Chadha diagram is used to determine the hydrochemical facies of groundwater. The diagram consists of four fields, representing four types of hydrogeochemical processes (Fig. 4). All the samples studied belong to Ca–Mg–Cl type water. This field indicates reverse ion exchange (Ca, Mg, Cl) processes (Kamel et al. 2013). In this zone, the strong acid anions (Cl^- and SO_4^{2-}) exceed the weak acid anions (HCO_3^-). In addition, the alkaline ions (Ca^{2+} and Mg^{2+}) bypass the alkalis (Na^+ and K^+). The results from the Chadha diagram corroborate the results obtained from the Piper diagram that they gave the same groundwater hydrochemical facies, which are dominated by the water type ($SO_4^{2-} - Cl^- - Ca^{2+} - Mg^{2+}$).

Overall, the waters of the Maadher plain have dominant hydro-chemical facies of sulfate–chloride-calcium-nitrate ($SO_4^{2-} - Cl^- - Ca^{2+} - NO_3^-$type water) and have a very remarkable tendency towards salinization. This is due to the presence of high proportions of the sum ($SO_4^{2-} + Cl^- + NO_3^-$) and ($Ca^{2+} + Na^+ + Mg^{2+}$).

Identification of water–rock interaction

The Gibbs diagram was used to establish the relationship between the water composition and the lithological characteristics of the aquifer (Ehya and Saeedi 2019; He et al. 2019). Gibbs divided the corresponding controlling factors of groundwater into three types: evaporation dominance, rock dominance, and precipitation dominance (Gibbs 1970).

Gibbs diagram represents the ratios of ($Na^+/(Na^+ + Ca^{2+})$) and ($Cl^-/ (Cl^- + HCO_3^-)$) as a function of total dissolved solids (TDS), see Fig. 4. The ratios of Na^+ are low relative to Ca^{2+} ratios; Cl^- ratios are a major contributor to high groundwater salinity (all samples exceed 0.6). The groundwater samples are in the zone of evaporation dominance, implying that evaporation is the main determinant of the chemical evolution of groundwater.

In Fig. 5a, the relationship between Ca^{2+} and SO_4^{2-} shows that the majority of the samples are close to the bisector line. Most of the samples are located above the dissolution line and indicate an excess of Ca^{2+}, suggesting a dissolution of carbonates. The fall of samples from wells 5, 17, 21, 26, and 33 below the bisector indicates a Ca^{2+} deficit, suggesting carbonate precipitation. The evaporation process is also important for controlling groundwater chemistry. In Fig. 5b is the plot of Ca^{2+} versus Na^+, all samples fall above the bisecting line except well 17, suggesting that halite dissolution affects salinity in these wells. According to Fig. 5c, groundwater mineralization is controlled, in addition to the mineral dissolution, by reverse ion exchange with clay minerals present in aquifers. The carbonate and silicate-weathering index shown in Fig. 5d shows that all samples lie above the bisecting line, indicating that the water samples are bound to carbonate rock.

Irrigation purposes

The collected groundwater samples were assessed for irrigation uses using different indices; the results are illustrated in Table 4. According to the TH (total hardness) values, 60.60% of samples present a soft water quality (TH < 75), and 36.36% of samples come moderately hard category. Finally, a hard water category of 3% represented in well 17. The %Na indicates that 72.72% of all samples are excellent for irrigation, and 24.24% of all samples are in the good category for irrigation. According to the SAR values, all samples of the aquifer present excellent water (SAR < 10).

Water quality indices

The water quality indices were applied to assess the quality of groundwater intended for drinking in the Maadher region, where the results are presented in Fig. 6. The calculated WQI values of 33 wells ranged from 61.47 to 310.62. The WQI indicated that the majority of the wells with 77.75% were in the poor water category and only well 13 contains good water. On the other hand, wells 1, 2, 3, 10, 19, and 23 are characterized by a very poor water category with 18.18%. Well 16 is classified in the category of not suitable for drinking water. These high WQI values found are due to high concentrations of sulfate, chloride, calcium, and nitrate.

The CCME-WQI gave similar results with arithmetic WQI, where the majority of the studied samples belonged to the marginal category with a 57.57%, and 36.36% of the samples belonged to the poor water category. The wells 13 and 26 belong to the good and fair categories, respectively.

Figure 6 shows the WQI and CCME-WQI values of the samples studied. These indices gave similar results, clearly noticeable in wells 5, 10, 16, 19, 23, 29, 4, 13, and 26.

The correlation matrix calculated between the physicochemical parameters and the water quality indices has been summarized in Table 5. For the arithmetic WQI, the strong correlation noted with the main parameters (EC, TH, Cl^-, SO_4^{2-}, Na^+, Ca^{2+}, Mg^{2+}, NO_3^-). On the other hand, a weak correlation was observed with NO_2^-, K^+, HCO_3^-, and pH. This case can be explained by the fact that the higher the concentrations of the main parameters, the higher the values of AWQI and the lower the water quality becomes.

Fig. 5 **a** Plot of SO_4^{2-} against Ca^{2+}. **b** Plot of Na^+ against Cl^-. **c** Plot of Na^+ against $(Ca^{2+}+Mg^{2+})$. **d** Plot of $(HCO_3^-+SO_4^{2-})$ against $(Ca^{2+}+Mg.^{2+})$
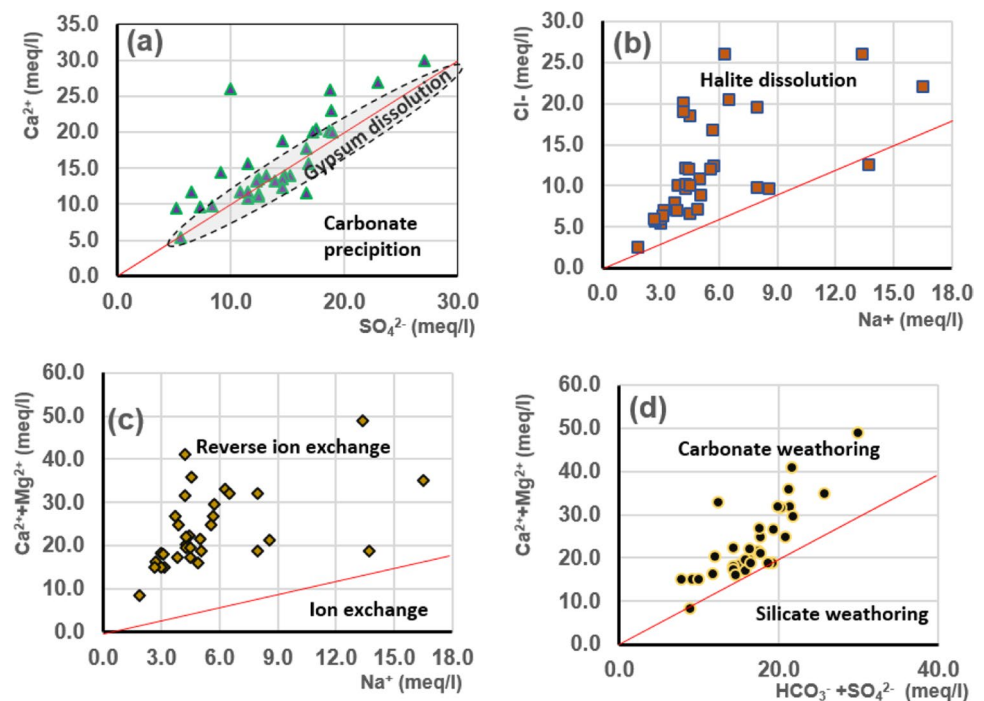
Table 4 Irrigation quality indices of Maadher aquifer

	Range	Classification	Nbr of samples	% of samples
Total Hardness (TH)		Soft	20	60.60%
	75–150	Moderately hard	12	36.36%
	150–300	Hard	1	3.03%
	> 300	Very hard	-	-
Percent sodium (%Na)	< 20	Excellent	24	72.72%
	20–40	Good	8	24.24%
	40–60	Permissible	1	3.03%
	60–80	Doubtful	-	-
	> 80	Unsafe	-	-
Sodium absorption ratio (SAR)	< 10	Excellent	All samples	100%
	10–18	Good	-	-
	18–26	Doubtful	-	-
	> 26	Unsuitable	-	-
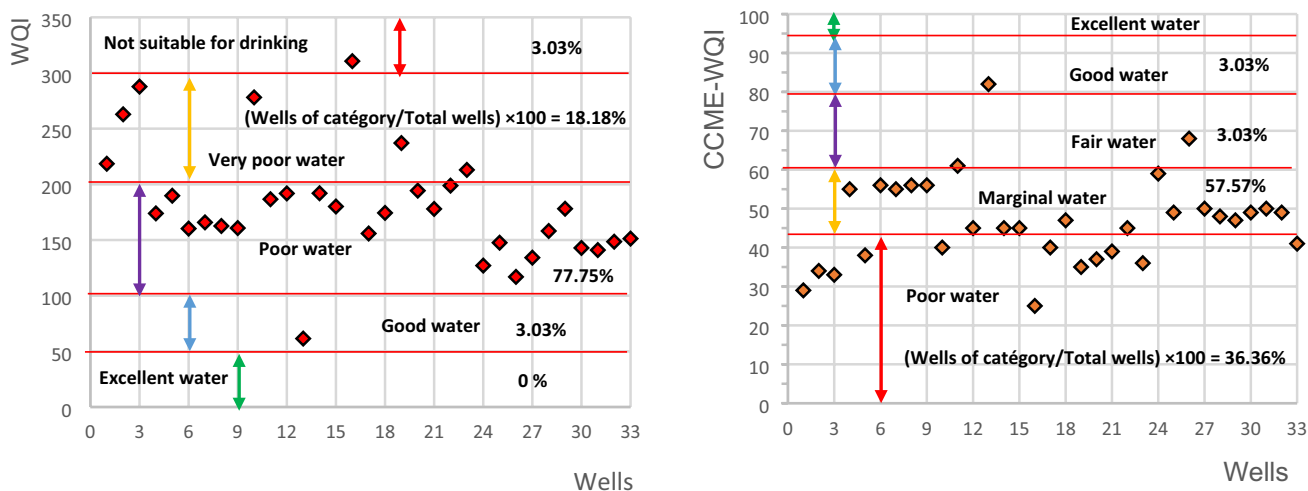
Fig. 6 Comparison between WQI and CCME-WQI results of groundwater samples studied

Table 5 Correlation between the physicochemical parameters and water quality indices

Index	pH	EC	Ca^{2+}	Mg^{2+}	HCO_3^-	Cl^-	SO_4^{2-}	TH	NO_3^-	Na^+	K^+	NO_2^-
WQI	−0.17	0.87	0.89	0.60	−0.41	0.82	0.63	0.85	0.565	0.51	0.49	0.23
CCME-WQI	0.27	−0.80	−0.78	−0.67	0.22	−0.72	−0.79	−0.83	−0.19	−0.55	−0.64	−0.29

For CCME-WQI, there is a strong inverse correlation with the main parameters (EC, Ca^{2+}, Mg^{2+}, Cl^-, SO_4^{2-}, TH, Na^+, K^+), a weak correlation with HCO_3^- and pH, NO_3^- and NO_2^-. The inverse correlation shows that the lower the concentrations of physicochemical parameters in the water, the higher the CCME-WQI values, the more the water quality improves, and vice versa.

Figure 7 displays the values for the two proposed indices calculations (WQI, CCME-IQE). Using two techniques, ordinary kriging and IDW, spatial distribution maps of index

values were created. While the index distributions yielded results that were generally comparable, the IDW method displayed greater local variation than the ordinary kriging method. The outcome demonstrates that the groundwater categories and groundwater flow are related (south to north). From the south to the north of the Maadher region, the groundwater category was good and fair, then poor. The poor category can be found in the area of Maadher and in the plain's northern region, specifically at the level of wells 1, 2, 3, 16, 17, and 19.
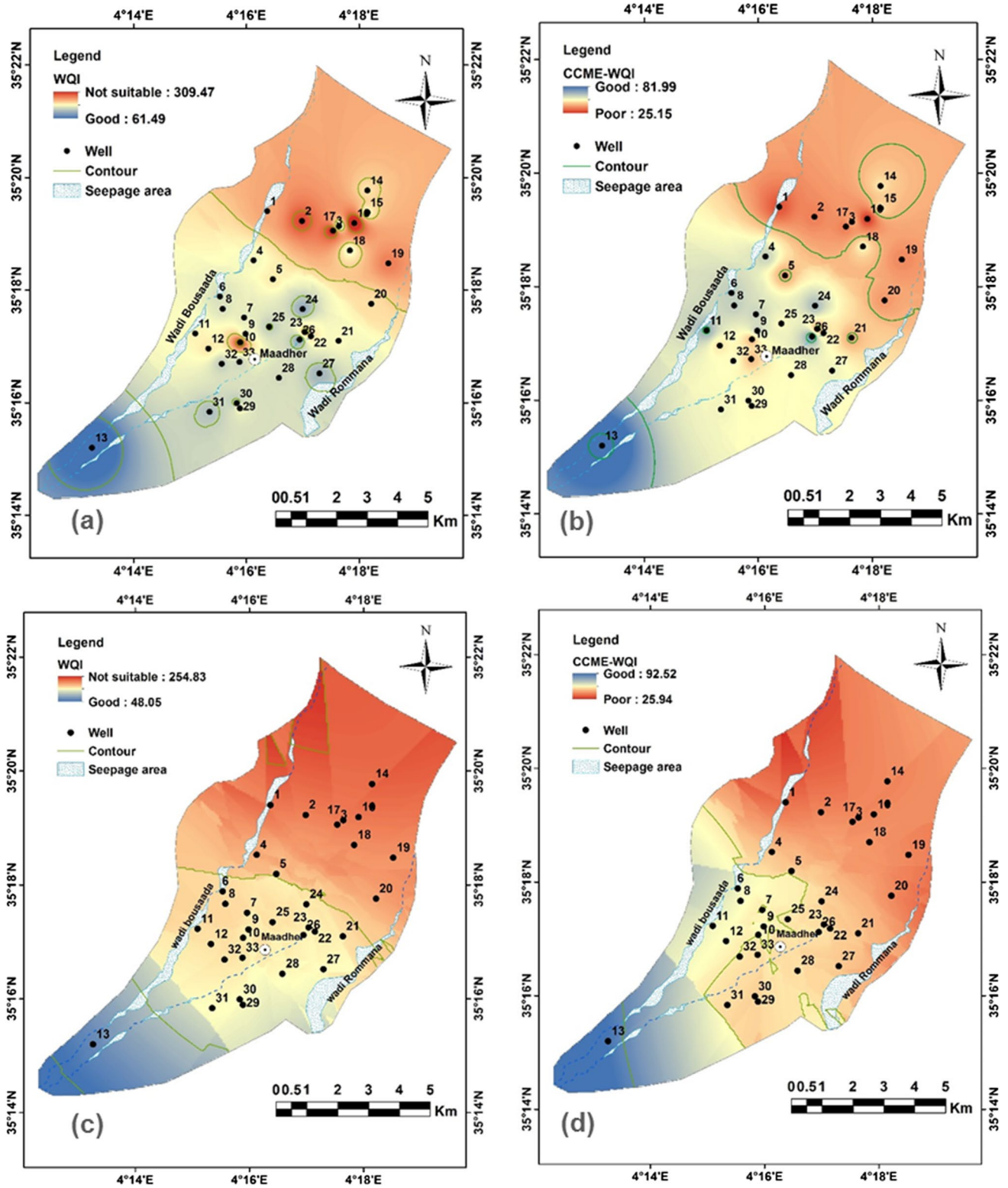
Fig. 7 Spatial distribution map of water quality indices (WQI, CCME-WQI). **a** and **b** Using IDW method. **c** and **d** Using ordinary kriging method

Spatial interpolation of principal physicochemical parameters using ordinary kriging

Interpolation by the ordinary kriging method shows the spatial distributions of the main quality parameters in the Maadher plain (Figs. 8 and 9). The spatial interpolations of Ca^{2+}, Mg^{2+}, Cl^-, and SO_4^{2-} have a similar distribution, a strong correlation between these parameters and EC. The direction of underground flow has an influence on the spatial distributions; where the concentrations are high (exceeding drinking water standards) in the northeast of the plain compared to the concentrations measured in the positions south and southwest of the Maadher plain (Fig. 8).

The spatial interpolations of Na^+, NO_3^-, NO_2^-, and HCO_3^- (Fig. 9) take different distributions compared to the first distributions; because wells 3, 16, and 17 have high Na^+ concentrations (exceeding drinking water standards). NO_3^- concentrations exceed the standards in most samples, but they are relatively low in the south and south-east compared to those in the northwest of the Maadher plain, and in particular, concentrations are high along the wadi of Bousaada (Fig. 9b). The reason for these high NO_3^- concentrations can be attributed to agricultural activities (synthetic and animal fertilizers) and the pollution of Bousaada Wadi, which serves as a dumping ground for local inhabitants. As for NO_2^- (Fig. 9c), all samples contain very weak concentrations. It
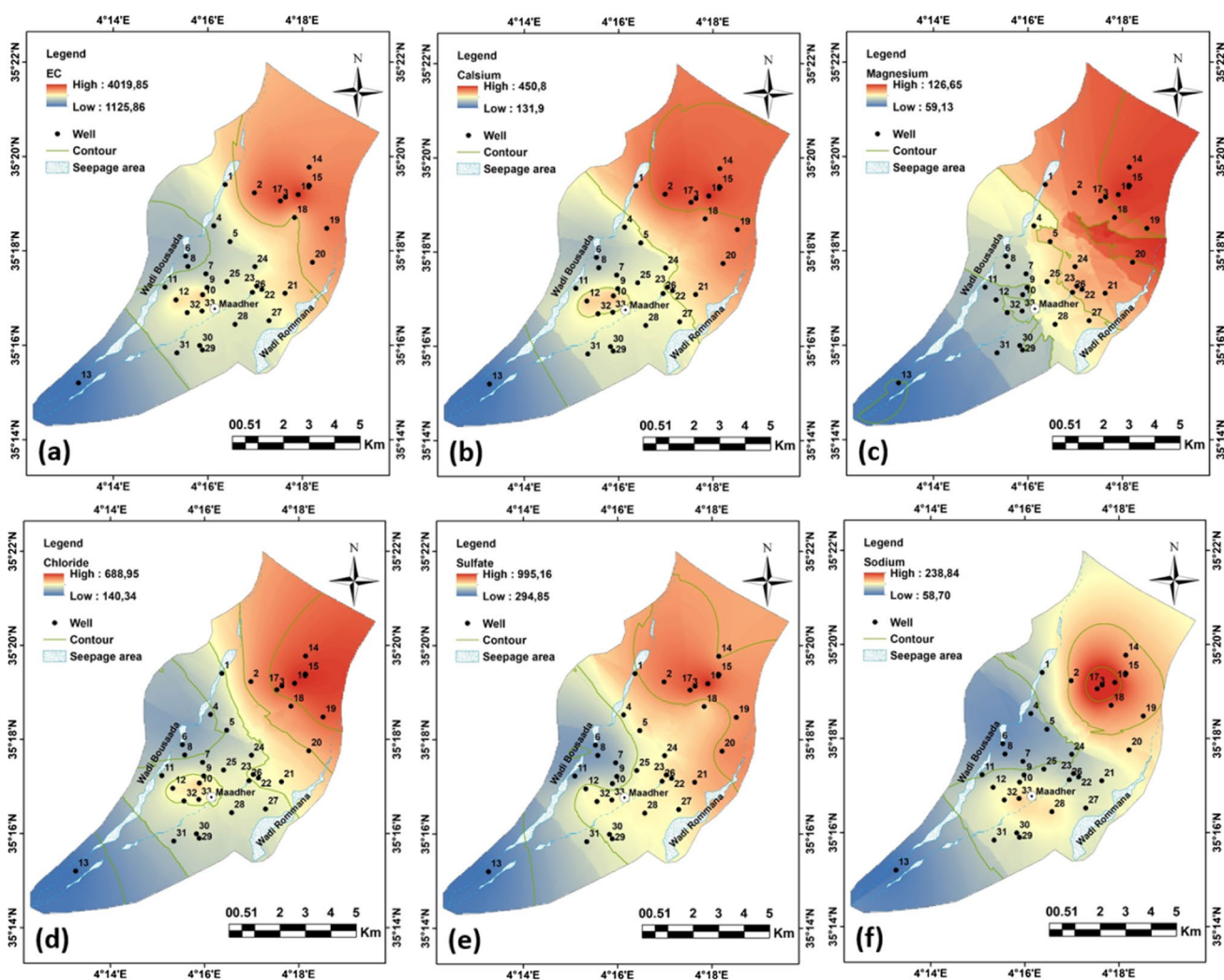

Fig. 8 Spatial distribution maps of EC, Ca^{2+}, Mg^{2+}, Cl^-, SO_4^{2-} and Na^+ using ordinary kriging method
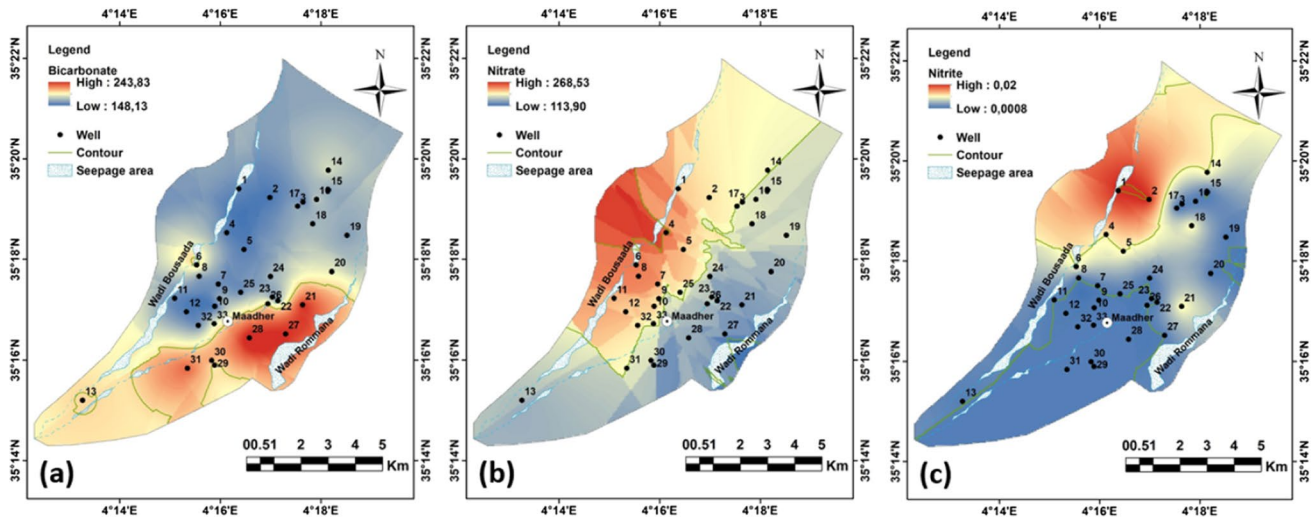
Fig. 9 Spatial distribution maps of HCO_3^-, NO_3^- and NO_2^- using ordinary kriging method

has an opposite spatial distribution of NO_3^-. This can be explained by the occurrence of the nitrification process; that is, the presence of favorable conditions that help to completely convert NO_2^- and NH_4^+ into nitrates. In addition, the spatial distribution of HCO_3^- is different from those of other quality parameters (Fig. 9a) and with the absence of direction of flow whose concentrations are low in the north and center of the Maadher plain and high in the south, notably in wells 21, 26, 27, 28, 3, and 6. This case can be explained by that during the process of denitrification, carbon is used as an electron donor (Wild et al. 2018). Therefore, we note that bicarbonate has opposite distributions of nitrate as well.

Technically, we used ArcGIS software to apply ordinary kriging to the dataset, using the spherical and Gaussian semi-variogram models because we found that they better fit the data. The Gaussian model for quality indices and the spherical model for quality parameters.

Interpreting a variogram's nugget, sill, or range is not particularly crucial. All of these are model parameters, even though some variogram models do not have a range and others only have an "effective" range. The nugget/sill ratio of kriging geostatistics indicates the degree of spatial variability that is affected by both structural/inherent and stochastic factors. A lower nugget/sill ratio indicates that structural factors (e.g., geological factors) play an important role in spatial variability. A higher nugget/sill ratio indicates that the spatial variability is mainly caused by stochastic factors (e.g., cropping systems and other human activities). The range is an indication of the proposed sampling distance from observation to observation.

The nugget-to-sill ratio reveals how spatially dependent certain variables are. For model explanation, three categories are used: strong spatial dependence is demonstrated by a ratio of less than 25%; moderate spatial dependence

Table 6 Statistical description of the saturation index for all minerals in groundwater samples

Mineral	Phase	Range	Mean $\pm$ SD
Anhydrite	$CaSO_4$	-1.52–0.59	-0.99 ± 0.22
Aragonite	$CaCO_3$	-0.04–0.82	**0.31** ± 0.16
Calcite	$CaCO_3$	0.11–0.97	**0.46** ± 0.17
CH_4 (g)	CH_4	-73.19–65.68	-68.54 ± 1.49
CO_2 (g)	CO_2	-3.11–-2.12	-2.54 ± 0.19
Dolomite	$CaMg (CO_3)_2$	0.05–1.64	**0.61** ± 0.31
Gypsum	$CaSO_4{:}2H_2O$	-1.11–-0.18	-0.59 ± 0.22
H_2 (g)	H_2	-24.33–-22.71	-23.30 ± 0.33
H_2O (g)	H_2O	-1.78–-1.75	-1.76 ± 0.01
Halite	NaCl	-7.00–-5.20	-6.03 ± 0.39
O_2 (g)	O_2	-41.41–-38.06	-40.04 ± 0.68
Sylvite	KCl	-7.45–-6.27	-6.75 ± 0.27

is shown by a ratio of between 25 and 75%; weak spatial dependence is demonstrated by a ratio of more than 75%.

Saturation index

The thermodynamic calculations of the saturation index for the groundwater samples are given in Table 6. All wells have similar values of the saturation index. The result indicates that the solid mineral phases of the groundwater samples such as anhydrite, gypsum, halite, and sylvite were undersaturated, implying that more solid phases or minerals must dissolve in the groundwater (meaning it tends to increase the concentrations of its chemical constituents in the water). Aragonite, calcite, and dolomite minerals were oversaturated, indicating more of the minerals need precipitation from water, it means that groundwater contains high concentrations of SO_4^{2-}, Ca^{2+}, and Mg^{2+}.

Carbonate minerals (aragonite, calcite, and dolomite) and sulfate minerals (gypsum and anhydrite) followed by (halite and sulfite) were the most common mineral phases that influenced the chemical composition of water resources in the study area, as shown in Fig. 10. The carbonate mineral saturation index of the dolomite was oversaturated, this oversaturation increased from wells 1, 5, 6, 12, 14, 15, 16, 24, and 26 while it decreased in the other wells; the same remark for aragonite and calcite. Sulfate minerals were undersaturated, but undersaturation increased (near 0) in wells 1, 2, 3, 12, 15, 16, 19, 20, and 23; the same remark was noted for halite and sylvite. During hydrogeochemical processes, carbonate

minerals (aragonite, calcite, and dolomite) are more likely to precipitate, while sulfate minerals (gypsum and anhydrite) as well as (halite and sylvite) are more likely to dissolve.

The SI plot of carbonate minerals such as aragonite, calcite, and dolomite with ($Ca^{2+} + HCO_3^-$) has been shown in Fig. 11a, and all samples indicated oversaturation except for well 33 which is undersaturated with aragonite. In Fig. 11b, the relationship between magnesium as a function of aragonite, calcite, and dolomite shows that all samples are oversaturated with these minerals, indicating that these phases tend to precipitate calcium and magnesium from water. The SI plot between sulfur minerals and SO_4^{2-} in groundwater.

Fig. 10 Saturation index of common minerals in the Maadher region: (aragonite, calcite, and dolomite), sulfate (gypsum and anhydrite), halite and sylvite in the water samples
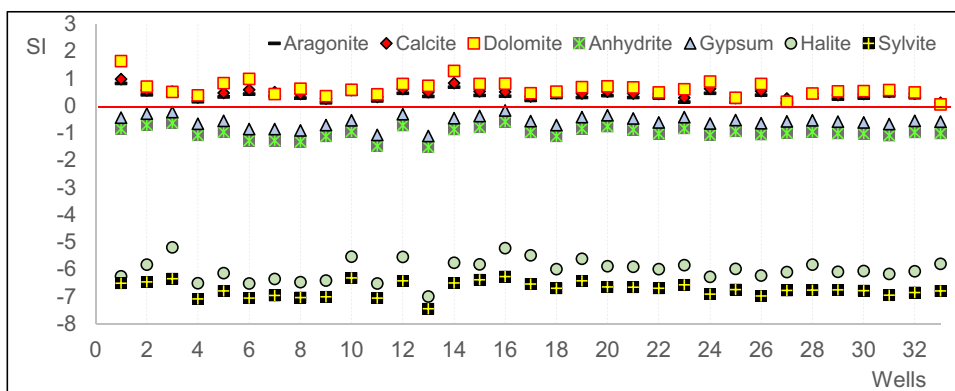

Fig. 11 **a** Plots of $Ca^{2+} + HCO_3^-$ vs. saturation indices of carbonate minerals. **b** Plots of Mg^{2+} vs. saturation indices of aragonite, calcite and dolomite
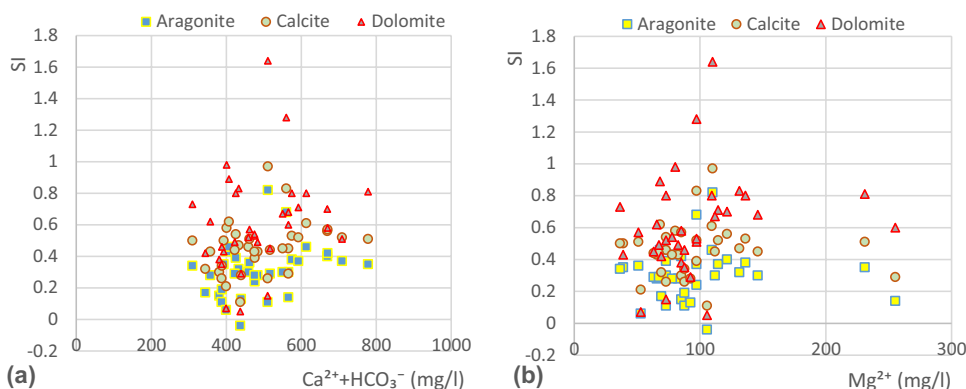

Fig. 12 **a** Plots of SO_4^{2-} vs. saturation indices of Gypsum and Anhydrite. **b** Plots of Cl^- vs. saturation indices of Halite and Sylvite minerals
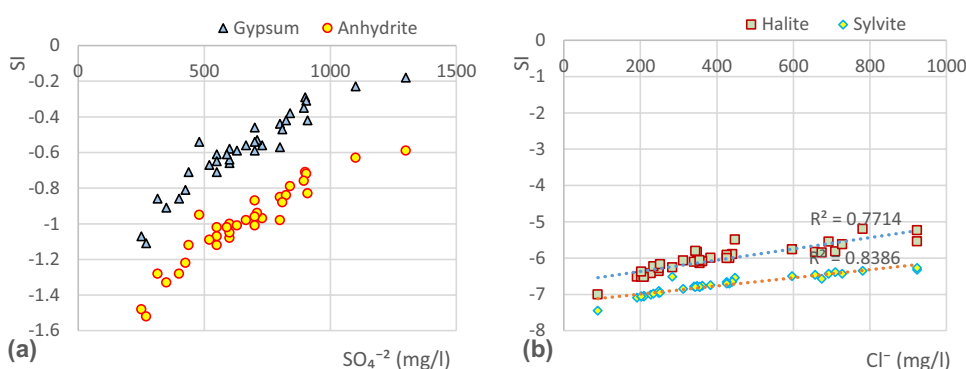
Figure 12a shows that the water samples are undersaturated, this suggests that if these minerals are present, they will be dissolved in groundwater and increase the concentration of SO_4^{2-}. Figure 12b illustrates the SI of halite (NaCl) and sylvite (KCl) in relation to the Cl^- concentration in water samples. The SI is strongly undersaturated (below zero), suggesting that halite and sylvite dissolve in groundwater and increase the concentration of Na^+, Cl^-, and K^+. The good linear correlation of Cl^- with halite and sylvite for the samples was indicated by the regression coefficient $R^2 = 0.84$ and $R^2 = 0.73$, respectively.

Conclusion

The primary source of water for domestic use and irrigation is the Maadher plain. Due to the presence of anthropogenic factors and the excessive use encouraged by climate change, the quality and quantity of this resource have significantly declined. This study examined the evaluation of groundwater quality using hydrogeochemistry and water quality indices (WQI, CCME-WQI) to identify wells, assess more mineralization, and assess contamination. The variation in water quality is now more understandable thanks to the use of the GIS spatial distribution in this study along with ordinary kriging and IWD techniques. The work that was presented can be summarized as follows:

- The concentrations of SO_4^{2-}, Cl^-, NO_3^- and Ca^{2+} exceeded WHO standard limits for drinking water; the groundwater belongs to hydrochemical facies sulfate–chloride-nitrate-calcium type water.

    - Since all samples from the Maadher zone are acceptable according to irrigation indices, the drinking water quality indices (WQI, CCME-WQI) place the zone's northern portion in the poor category, its southern portion in the good category, and its center in the medium category.
- Using the GIS technique, spatial interpolations of Ca2+, Mg2+, Cl^-, and SO42- reveal a similar distribution. These spatial distributions are in accordance with the direction of underground flows, with high concentrations in the north and low concentrations in the south of the study area. Aside from the bicarbonate and nitrate concentrations, which were higher close to the Bousaada wadi depression.
- The present study's findings showed that excessive agricultural practices and inflows from the Bousaada wadi, two examples of anthropogenic activities, had a significant negative impact on the quality of groundwater in the study area.
- The minerals anhydrite, gypsum, halite, sylvite, aragonite, calcite, and dolomite precipitate and dissolve in groundwater to form its chemical composition. We also consider the effects of regional climate change, such as the increase in temperatures and decrease in precipitation, which increase the need for water.
- Since the CCME-WQI has demonstrated its effectiveness on groundwater by producing results comparable to the WQI, the techniques used in the assessment of groundwater quality have given satisfactory results. The ordinary kriging and IDW interpolation methods made it possible to concretize the hypotheses presented through precise and interpreted maps of the phenomena that occur in the study area. Future work will focus on the choice of interpolation techniques as well as the criteria for applying variogram models for a good representation of GIS.

Declarations

Ethical approval Not applicable.

Consent to participate Not applicable.

Consent for publication Not applicable.

Competing interests The authors declare no competing interests.

References

Abdesselam S, Halitim A, Jan A, Trolard F, Bourrié G (2013) Anthropogenic contamination of groundwater with nitrate in arid regions: case study of southern Hodna (Algeria). Environ Earth Sci 70(5):2129–2141. https://doi.org/10.1007/s12665-012-1834-5

Ahmad S, Umar R, Arshad I (2019) Groundwater quality appraisal and its hydrogeochemical characterization Mathura City, Western Uttar Pradesh. J Geol Soc India 94(6):611–623. https://doi.org/10.1007/s12594-019-1368-5

Aissaoui D M (1989) Upper Jurassic paleogeography south of Chott El Hodna, Algeria. J Afr Earth Sci 9(3/4): 413–420. In French. https://doi.org/10.1016/0899-5362(89)90025-0

ANRH (2006) Modeling of the Hodna aquifer. Mission I: data collection, analysis and synthesis (in French). Tech. Rep., Agence nationale des ressources hydrauliques, Algérie

Askri H, Belmecheri A, Benrabah B, Boudjema A, Boumendjel K, Daoudi M Terkmani M (1995) Geology of Algeria. In Well Evaluation Conference Algeria 1–93

Aravinthasamy P, Karunanidhi D, Subba Rao N, Subramani T, Srinivasamoorthy K (2020) Irrigation risk assessment of groundwater in a non-perennial river basin of South India: implication from irrigation water quality index (IWQI) and geographical information system (GIS) approaches. Arab J Geosci 13(21):1–14. https://doi.org/10.1007/s12517-020-06103-1

Abdelshafy M, Saber M, Abdelhaleem A, Abdelrazek SM, Seleem EM (2019) Hydrogeochemical processes and evaluation of groundwater aquifer at Sohag City Egypt. Sci Afr 6:e00196. https://doi.org/10.1016/j.sciaf.2019.e00196

Belkhiri L, Tiri A, Mouni L (2020) Spatial distribution of the groundwater quality using kriging and co-kriging interpolations. Groundw Sustain Dev 11:100473. https://doi.org/10.1016/j.gsd.2020.100473

Boudiaf B, Dabanli I, Boutaghane H, Şen Z (2020) Temperature and precipitation risk assessment under climate change effect in Northeast Algeria. Earth Syst Environ 4(1):1–14. https://doi.org/10.1007/s41748-019-00136-7

Boudjemline F, Semar A (2018) Assessment and mapping of desertification sensitivity with MEDALUS model and GIS–Case study: basin of Hodna, Algeria. Journal of water and land development. DOI: https://doi.org/10.2478/jwld-2018-0002

Bahir M, Ouhamdouch S, Ouazar D et al (2020) Assessment of groundwater quality from semi-arid area for drinking purpose using statistical, water quality index (WQI) and GIS technique. Carbonates Evaporites 35:27. https://doi.org/10.1007/s13146-020-00564-x

CCME (2017) Canadian water quality guidelines for the protection of aquatic life: CCME Water Quality Index, User's Manual. The Canadian Council of Ministers of the Environment (CCME)

Chapman D (2021) Water quality assessments: a guide to the use of biota, sediments and water in environmental monitoring. CRC Press https://doi.org/10.1201/9781003062103

Derekov A M (1973) Hydrological studies in the Chott El Hodna basin. Technical report, FAO

Dougha M, Hasbaia M (2019) Contribution of the multivariate analysis and origin for groundwater quality of mixed aquifer in the M'sila plain (Algeria). Int J Hydrol Sci Technol 9(2):154–172. https://doi.org/10.1504/IJHST.2019.098160

El-Zeiny AM, Elbeih SF (2019) GIS-based evaluation of groundwater quality and suitability in Dakhla Oases Egypt. Earth Syst Environ 3(3):507–523. https://doi.org/10.1007/s41748-019-00112-1

Ehya F, Saeedi F (2019) Assessment of groundwater quality in the Garmez area (Southeastern Khuzestan province, SW Iran) for drinking and irrigation uses. Carbonates Evaporites 34:1443–1454. https://doi.org/10.1007/s13146-018-0481-7

El Mountassir O, Bahir M, Ouazar D, Ouhamdouch S, Chehbouni A, Ouarani M (2020) The use of GIS and water quality index to assess groundwater quality of krimat aquifer (Essaouira; Morocco). SN Appl Sci 2(5):1–16. https://doi.org/10.1007/s42452-020-2653-z

Fetter CW (2018) Applied hydrogeology. Waveland Press

Gibbs RJ (1970) Mechanisms controlling world water chemistry. Science 170(3962):1088–1090

Guiraud R (1973) The main features of the Hodna Chott basin Hydrogeology, Northern Algeria (in French). Publi Servi Géol 39:159–170

Guiraud R (1970) Quaternary morphogenesis of the Hodna region (Northern Algeria) (in French). In Annals of Geography. Persée-Portal of scientific journals in SHS 79(433):367–374

Ghazaryan K, Movsesyan H, Gevorgyan A, Minkina T, Sushkova S, Rajput V, Mandzhieva S (2020) Comparative hydrochemical assessment of groundwater quality from different aquifers for irrigation purposes using IWQI: a case-study from Masis province in Armenia. Groundw Sustain Dev 11:100459. https://doi.org/10.1016/j.gsd.2020.100459

Gao X, Su C, Wang Y, Hu Q (2013) Mobility of arsenic in aquifer sediments at Datong Basin, northern China: effect of bicarbonate and phosphate. J Geochem Explor 135:93–103. https://doi.org/10.1016/j.gexplo.2012.09.001

He X, Wu J, He S (2019) Hydrochemical characteristics and quality evaluation of groundwater in terms of health risks in Luohe aquifer in Wuqi County of the Chinese Loess Plateau, northwest China. Hum Ecol Risk Assess Int J 25(1–2):32–51. https://doi.org/10.1080/10807039.2018.1531693

Hu J, Zhu C, Long Y, Yang Q, Zhou S, Wu P, Hu X (2021) Interaction analysis of hydrochemical factors and dissolved heavy metals in the karst Caohai Wetland based on PHREEQC, cooccurrence network and redundancy analyses. Sci Total Environ 770:145361. https://doi.org/10.1016/j.scitotenv.2021.145361

Hussain Y, Ullah SF, Hussain MB, Aslam AQ, Akhter G, Martinez-Carvajal H, Cárdenas-Soto M (2017) Modelling the vulnerability of groundwater to contamination in an unconfined alluvial aquifer in Pakistan. Environ Earth Sci 76(2):1–11

Jalees MI, Farooq MU, Anis M, Hussain G, Iqbal A, Saleem S (2021) Hydrochemistry modeling: evaluation of groundwater quality deterioration due to anthropogenic activities in Lahore. Pakistan Environment Development and Sustainability 23(3):3062–3076. https://doi.org/10.1007/s10668-020-00703-3

Jampani M, Liedl R, Hülsmann S, Sonkamble S, Amerasinghe P (2020) Hydrogeochemical and mixing processes controlling groundwater chemistry in a wastewater irrigated agricultural system of India. Chemosphere 239:124741. https://doi.org/10.1016/j.chemosphere.2019.124741

Kim J, Lee KK (2022) Hydrogeochemical signatures for sustainable use of shallow groundwater as a thermal resource at groundwater–surface water mixing zone. Environmental Earth Sciences 81(11):1–13. https://doi.org/10.1007/s12665-022-10439-0

Li D, Gao X, Wang Y, Luo W (2018) Diverse mechanisms drive fluoride enrichment in groundwater in two neighboring sites in northern China. Environ Pollut 237:430–441. https://doi.org/10.1016/j.envpol.2018.02.072

Li C, Gao X, Wang Y (2015) Hydrogeochemistry of high-fluoride groundwater at Yuncheng Basin, northern China. Sci Total Environ 508:155–165. https://doi.org/10.1016/j.scitotenv.2014.11.045

Luo W, Gao X, Zhang X (2018) Geochemical processes controlling the groundwater chemistry and fluoride contamination in the Yuncheng Basin, China—an area with complex hydrogeochemical conditions. PLoS ONE 13(7):e0199082. https://doi.org/10.1371/journal.pone.0199082

Lu P, Zhang G, Apps J, Zhu C (2022) Comparison of thermodynamic data files for PHREEQC. Earth-Science Review 225:103888. https://doi.org/10.1016/j.earscirev.2021.103888

Mutlu E (2019) Evaluation of spatio-temporal variations in water quality of Zerveli stream (northern Turkey) based on water quality index and multivariate statistical analyses. Environ Monit Assess 191(6):1–14. https://doi.org/10.1007/s10661-019-7473-5

Obaid A N, Mohammed M J (2020) A comparison of topological kriging and area to point kriging for irregular district area in IRAQ. Journal of Mechanics of Continua and Mathematical Sciences. https://doi.org/10.26782/jmcms.2020.04.00009

Oseke FI, Anornu GK, Adjei KA, Eduvie MO (2021) Assessment of water quality using GIS techniques and water quality index in reservoirs affected by water diversion. Water-Energy Nexus 4:25–34. https://doi.org/10.1016/j.wen.2020.12.002

Pazand K, Khosravi D, Ghaderi MR, Rezvanianzadeh MR (2018) Identification of the hydrogeochemical processes and assessment of groundwater in a semi-arid region using major ion chemistry: a case study of Ardestan basin in Central Iran. Groundw Sustain Dev 6:245–254. https://doi.org/10.1016/j.gsd.2018.01.008

Panneerselvam B, Muniraj K, Thomas M, Ravichandran N (2021) GIS-based legitimatic evaluation of groundwater's health risk and irrigation susceptibility using water quality index, pollution index, and irrigation indexes in semi-arid region. In Groundwater resources development and planning in the semi-arid region (pp. 239–268). Springer, Cham

Rabeiy RE (2018) Assessment and modeling of groundwater quality using WQI and GIS in upper Egypt area. Environ Sci Pollut Res 25(31):30808–30817. https://doi.org/10.1007/s11356-017-8617-1

Rata M, Douaoui A, Larid M, Daouik A (2018) Spatial analysis of annual rainfall using ordinary kriging techniques and lognormal kriging in the Cheliff watershed. Algeria. Journal of Environmental Sciences, 1(1)

Rostami AA, Karimi V, Khatibi R, Pradhan B (2020) An investigation into seasonal variations of groundwater nitrate by spatial modeling strategies at two levels by kriging and co-kriging models. Journal of environmental management 270: 110843 10.1016/

Rashid A, Ayub M, Javed A, Khan S, Gao X, Li C, Nazneen S (2021) Potentially harmful metals, and health risk evaluation in groundwater of Mardan, Pakistan: application of geostatistical approach and geographic information system. Geosci Front 12(3):101128. https://doi.org/10.1016/j.gsf.2020.12.009

Rashid A, Guan DX, Farooqi A, Khan S, Zahir S, Jehan S, Khan R (2018) Fluoride prevalence in groundwater around a fluorite mining area in the flood plain of the River Swat, Pakistan. Sci Total Environ 635:203–215. https://doi.org/10.1016/j.scitotenv.2018.04.064

Rashid A, Farooqi A, Gao X, Zahir S, Noor S, Khattak JA (2020) Geochemical modeling, source apportionment, health risk exposure and control of higher fluoride in groundwater of sub-district Dargai Pakistan. Chemosphere 243:125409. https://doi.org/10.1016/j.chemosphere.2019.125409

Rashid A, Khan S, Ayub M, Sardar T, Jehan S, Zahir S, Ullah H (2019) Mapping human health risk from exposure to potential toxic metal contamination in groundwater of Lower Dir, Pakistan: application of multivariate and geographical information system. Chemosphere 225:785–795. https://doi.org/10.1016/j.chemosphere.2019.03.066

Radouane E M, Chahlaoui A, Maliki A, Boudellah A (2021) Assessment and modeling of groundwater quality by using water quality index (WQI) and GIS technique in meknes aquifer (Morocco). *Geology, Ecology, and Landscapes* 1-13 https://doi.org/10.1080/24749508.2021.1944797

Ramachandran A, Sivakumar K, Shanmugasundharam A, Sangunathan U, Krishnamurthy RR (2021) Evaluation of potable groundwater zones identification based on WQI and GIS techniques in Adyar River basin, Chennai, Tamilnadu India. Acta Ecologica Sinica 41(4):285–295. https://doi.org/10.1016/j.chnaes.2020.02.006

Singh P, Verma P (2019) A comparative study of spatial interpolation technique (IDW and kriging) for determining ground water quality. GIS and Geostatistical Techniques for Groundwater Science. Elsevier, Amsterdam, The Netherlands: 43–56

Selmane T, Dougha M, Hasbaia M, Ferhati A, Redjem A (2022) Hydrogeochemical processes and multivariate analysis for groundwater quality in the arid Maadher region of Hodna, northern Algeria. Acta Geochimica 41(5):893–909. https://doi.org/10.1007/s11631-022-00553-y

Shil S, Singh UK, Mehta P (2019) Water quality assessment of a tropical river using water quality index (WQI), multivariate statistical techniques and GIS. Appl Water Sci 9(7):1–21

Soltani AA, Bermad A, Boutaghane H, Oukil A, Abdalla O, Hasbaia M, Lefkir A (2020) An integrated approach for assessing surface water quality: Case of Beni Haroun dam (Northeast Algeria). Environ Monit Assess 192(10):1–17. https://doi.org/10.1007/s10661-020-08572-z

Taloor AK, Pir RA, Adimalla N, Ali S, Manhas DS, Roy S, Singh AK (2020) Spring water quality and discharge assessment in the Basantar watershed of Jammu Himalaya using geographic information system (GIS) and water quality Index (WQI). Groundw Sustain Dev 10:100364

Uddin MG, Nash S, Olbert AI (2020a) A review study of water quality index models and their use for assessing surface water quality. Ecol Ind. https://doi.org/10.1016/j.ecolind.2020.107218

Uddin MG, Olbert AI, Nash S (2020b) Assessment of water quality using Water Quality Index (WQI). Ecol Indic 85:966–982

Wilde F D (2010) Water-quality sampling by the US Geological Survey: standard protocols and procedures. US Geological Survey Fact Sheet. 312(2)

WHO (2011) Guidelines for drinking-water quality WHO (Ed.) Retrieved from http://www.who.int/water_sanitation_health/publications/2011/dwq_guidelines/en/

Wild LM, Mayer B, Einsiedl F (2018) Decadal delays in groundwater recovery from nitrate contamination caused by low O2 reduction rates. Water Resour Res 54(9996–10):012. https://doi.org/10.1029/2018WR023396

Wen D, Zhang F, Zhang E, Wang C, Han S, Zheng Y (2013) Arsenic, fluoride and iodine in groundwater of China. J Geochem Explor 135:1–21. https://doi.org/10.1016/j.gexplo.2013.10.012

Yilma M, Kiflie Z, Windsperger A, Gessese N (2018) Application of artificial neural network in water quality index prediction: a case study in Little Akaki River, Addis Ababa Ethiopia. Model Earth Syst Environ 4(1):175–187. https://doi.org/10.1007/s40808-018-0437-x